Energy Dissipations in Chlorosomes: Emission from the Q_y State Following Singlet−Singlet and Triplet−Triplet Annihilation Reactions in the Cylindrical Aggregate and Its Reversible Dissociation into the Piggy-Back Dimers

Yoshinori Kakitani,[†] Ferdy S. Rondonuwu,[†] Tadashi Mizoguchi,[‡] Yasutaka Watanabe,[†] and Yasushi Koyama*,[†]

Department of Chemistry and Department of Physics, Faculty of Science and Technology, Kwansei Gakuin University, 2-1 Gakuen, Sanda 669-1337, Japan, and Department of Bioscience and Biotechnology, Ritsumeikan University, Nojihigashi, Kusatsu 525-8577, Japan

Received: January 9, 2003; In Final Form: September 17, 2003

The excited-state dynamics of chlorosomes from *Chlorobium tepidum*, upon excitation above the Soret state, was examined by pump-and-probe time-resolved absorption spectroscopy in the subpicosecond to millisecond time region. Upon excitation using a 397-nm, 0.10-ps pulse, the singlet−singlet annihilation (reaction I) as well as the singlet homofission followed by the triplet−triplet annihilation (reaction II) were seen as bimolecular reactions in the subpicosecond to picosecond time regime. Upon excitation using a 355-nm, 12-ns pulse, the dissociation of chlorosomes into the piggy-back dimers (reaction III) was seen in submicroseconds; the chlorosome structure was reorganized within ∼20 ms. Thus, the cylindrical aggregate structure of chlorosomes facilitates efficient radiative-energy dissipation either through the initial stimulated emission from the Q_y state (after reaction I) or through the delayed stimulated emission from the Q_y state (after reaction II). The excess thermal energy that is produced by the internal-conversion and vibrational-relaxation processes seems to be dissipated during the instantaneous dissociation of the aggregate structure (after reaction III).

Introduction

Green sulfur bacteria, *Chlorobiaceae*, and green filamentous bacteria, *Chloroflexaceae*, contain closely related antenna complexes called "chlorosomes". Chlorosomes in *Chlorobium (Chl.) tepidum* consist of rod elements mainly made up of $\sim 10^3$ bacteriochlorophyll (BChl) *c*, a small amount of carotenoid (chlorobactene), and a surrounding lipid monolayer that contains the BChl *a* baseplate protein; the latter provides the connection of chlorosomes to the cytoplasmic membrane containing the reaction centers (RCs; see refs 1−4 for reviews). The kinetics and pathways of energy transfer in the rod elements and in the membrane proteins have been studied extensively by means of picosecond and subpicosecond time-resolved absorption spectroscopy. It has been shown that the light energy harvested by BChl *c* in the rod is transferred to the baseplate BChl *a* in the envelope. Hereafter, we will confine ourselves to describing the excited-state and the ground-state dynamics in the rod by the use of chlorosome samples containing a minimum amount of BChl *a*. In the rod, the BChl *c* molecules are self-organized as an aggregate through pigment−pigment intermolecular interactions, which presumably include the coordination of the 3-hydroxyethyl oxygen to the central magnesium atom and hydrogen bonding by the use of the 3-hydroxyethyl OH and the keto C═O groups. Concerning the basic structural motif of the stacking of BChl *c* macrocycles, two different models have been proposed: one consisting of stacked monomers to form an inclined column,[5−7] and the other consisting of stacked "piggy-back dimers" to form such a column.[8] The structure of the piggy-back dimers in methylene chloride solution has been proved by NMR spectroscopy.[9−11] It has been generally accepted that the two-dimensional network of the BChl *c* aggregate forms a cylindrical structure (see Figure 8 of ref 1).

Concerning the excited-state dynamics in the aggregate, extensive studies have been made by means of fast laser spectroscopy. The following are some examples: (i) One of the most recent subpicosecond time-resolved absorption studies[12] has found that the initial Q_y bleaching of the BChl *c* aggregate in chlorosomes is 7−8 times larger than that of BChl *a*. This was ascribed to a high extinction coefficient originating from the delocalized excitonic excitation. (ii) A femtosecond time-resolved absorption study identified three decay components, that is, ∼100 fs, ∼2 ps, and ∼10 ps;[13] the last component was associated with the BChl *c* to BChl *a* singlet energy-transfer reaction.[13,14] (iii) A previous picosecond time-resolved absorption study showed that increasing photon density for excitation caused a decrease in the magnitude of initial bleaching, keeping the time profile of recovery almost identical. This observation suggests the presence of annihilation processes faster than the time resolution of 2 ps.[14] On the basis of those results, it has been suggested that strong electronic coupling in the cylindrical aggregate may cause a set of delocalized, excitonic excitations with a certain coherence length and facilitates extremely efficient migration of the singlet and triplet excitations. Thus, the aggregate structure is considered to be advantageous in pursuing both the light-harvesting and the photoprotective functions. It can transfer the delocalized excitations on the large aggregate structure and also facilitate efficient annihilation reactions.

Concerning a more specific photoprotective function, it has been shown that a trace of radical cation is present in the aggregate and quenches the singlet excitation: (i) The Q_y

* To whom correspondence should be addressed. Fax: +81-79-565-9077. Phone: +81-79-565-8408. E-mail: ykoyama@kwansei.ac.jp.
[†] Kwansei Gakuin University.
[‡] Ritsumeikan University.

10.1021/jp0300288 CCC: $25.00
Published on Web 11/27/2003

lifetime and the energy-transfer efficiency strongly depend on the redox potential;[15,16] when chlorosomes were reduced, the fluorescence lifetime extended to tens of picoseconds in *Chl. tepidum*.[17] (ii) The presence (absence) of radical cations in the nonreduced (reduced) chlorosomes was established by electron paramagnetic resonance spectroscopy.[17] (iii) It has been proposed that the mechanism of quenching the S_1 state should prevent the reduction of oxygen (O_2), if any, into the superoxide radical anion ($O_2^{\bullet-}$) by low-potential electron acceptors in the RC.[16,18]

In the present investigation, we examined how the aggregated structure in chlorosomes can dissipate the excess energy when a large number of high-energy photons are applied. The conditions were nonphysiological, but we tried to thoroughly investigate all the possible mechanisms of energy dissipation. Then, we will be able to discuss such dissipation mechanisms should be in operation, or not, under the physiological conditions. To the knowledge of the authors, no such strategy has yet been taken. Under those excitation conditions, reactions among the singlet and triplet excitations, including singlet−singlet annihilation as well as a combination of singlet homofission and triplet−triplet annihilation, need to be considered as the intrinsic properties of the aggregate structure.

Another important issue is how the excess thermal energy that is generated as the results of the internal-conversion and vibrational-relaxation processes can be dissipated. The rigid framework of the aggregate structure is obviously disadvantageous to achieve this thermal-energy dissipation, and, therefore, some loosening (melting) of the structure may be advantageous for increasing the vibrational degrees of freedom to facilitate the more efficient dissipation of thermal energy.

On the basis of these considerations, we have addressed the following two specific questions: (1) Can the previously mentioned excited-state reactions actually serve as the mechanisms of efficient quenching of the singlet and the triplet excitations? (2) Is there any change in the aggregate structure as a mechanism of efficient dissipation of the thermal energy?

Materials and Methods

Preparation of Chlorosome Samples. *Chl. tepidum* ATCC49652 was grown in the medium of Wahlund et al.[19] under anaerobic conditions in dim light. The cells were washed with a buffer solution containing 10 mM potassium phosphate, 10 mM sodium L-ascorbate, and 2 M NaSCN (pH 7.4) and then disrupted four times by the use of a French press (pressure, 1100−1200 kgf·cm^{-2}). The suspension was centrifuged at 20 000*g* for 45 min, and the supernatant was suspended in 15% sucrose and purified by sucrose density-gradient centrifugation (180 000*g* for 18 h) using 0, 10, 15 (containing the suspension), 25, 40, and 50% sucrose layers. A fraction showing the minimum BChl *a* absorption originating from the Fenna−Matthews−Olson (FMO) protein was collected as crude chlorosomes. It was then diluted with 2 vol of 50 mM Tris-HCl buffer containing 1 mM ethylenediaminetetraacetic acid (EDTA; pH 8.0) and centrifuged again at 200 000*g* for 1 h to remove sucrose and FMO. This set of purification procedures was repeated two more times to obtain what we call "native" chlorosomes.

"Carotenoid (Car)-depleted" chlorosomes were prepared by the same procedure from the cells grown in the previously described medium, to which 37−40 μg/mL hydroxybiphenyl was added;[20,21] the amount of carotenoids was reduced to 45%. "Reduced" chlorosomes were obtained by adding 20 mM $Na_2S_2O_4$ to the native chlorosome suspension. The native chlorosome suspension was bubbled through nitrogen or air for 30 min to partially disrupt the aggregate structure of chlorosomes.

Isolation of BChl *c* Isomers. A mixture of BChl *c* isomers was extracted with methanol from the cells of *Chl. tepidum* in the dark under a nitrogen atmosphere. The extract was fractionated between petroleum ether plus diethyl ether (1:2 v/v) and a NaCl-saturated aqueous solution. In a second extraction procedure, acetone was used instead. Both the methanol and acetone extracts were filtered over NaCl, and then, the solvents were evaporated in vacuo. The residual pigments were placed on a crystalline cellulose filter, and carotenoid and BChl *a* were removed with *n*-hexane; then, the residual crude BChl *c* isomers were eluted with acetone. After removal of acetone by evaporation, the crude BChl *c* component was dissolved into a minimum amount of methanol and subjected to C18 reversed-phase column chromatography (column, a Sep-Pack Plus C18 Cartridge, WATERS; and eluent, methanol) to remove lipids and other contaminants, resulting in an isomeric mixture of BChl *c*.

Subpicosecond to Nanosecond and Submicrosecond to Millisecond Time-Resolved Absorption Spectroscopy. The isomeric mixture of BChl *c* was dissolved in methanol (spectral grade, Kishida Chemicals) at a concentration of 1×10^{-4} M to form monomers. The native or modified chlorosomes were suspended in a 50 mM Tris-HCl buffer containing 1 mM EDTA (pH 8.0) to an optical density of $OD_{400} = \sim 4.5$ cm^{-1}. The sample solution or suspension was circulated between a flow cell (optical path length, 1 mm) and an ice-cooled reservoir (15 mL) by the use of a pump (linear speed in the cell, 7 cm·s^{-1}). The stationary-state electronic absorption spectra were recorded on HITACHI U-2000 spectrophotometer before and after each measurement; no photodegradation was identified at all.

Subpicosecond to nanosecond time-resolved absorption spectra were recorded by the use of a setup described previously.[22] A 397-nm, 0.10-ps, and 1-kHz pulse was used for pumping, the autocorrelation between the pump and the white-continuum probe pulse being ~0.13 ps full width at half-maximum. The power of the pumping pulse was 6 μJ·pulse^{-1} (4×10^{14} photon·cm^{-2}·pulse^{-1}) in the "high photon-density" excitation, whereas it was 1 μJ·pulse^{-1} (7×10^{13} photon·cm^{-2}·pulse^{-1}) in the "low photon-density" excitation. A total of 400 pairs of pulses were accumulated at each delay time.

Submicrosecond to millisecond time-resolved absorption spectra were recorded by using a setup described previously.[23] A 355-nm, 12-ns pulse was used for pumping with a power of 3.5 mJ·pulse^{-1} (1.6×10^{17} photon·cm^{-2}·pulse^{-1}), that is, excitation with "extremely high photon density", whereas a white-continuum pulse from a Xe flash lamp was used for probing; the gate width was 80 ns. At each delay time, the spectral data of 20 pairs of pump and probe pulses were accumulated in the 400−600-nm region, whereas those of 40 pairs of pump and probe pulses were accumulated in the 600−800-nm region.

In some cases, the time-resolved data matrix was analyzed by the use of singular-value decomposition (SVD) and subsequent global fitting based on a target model, as described previously.[24]

Results and Discussion

Preliminary Considerations. (A) Characterization of the Samples. To elucidate the unique excited-state properties of the aggregate structure in native chlorosomes, the following samples were examined for comparison:

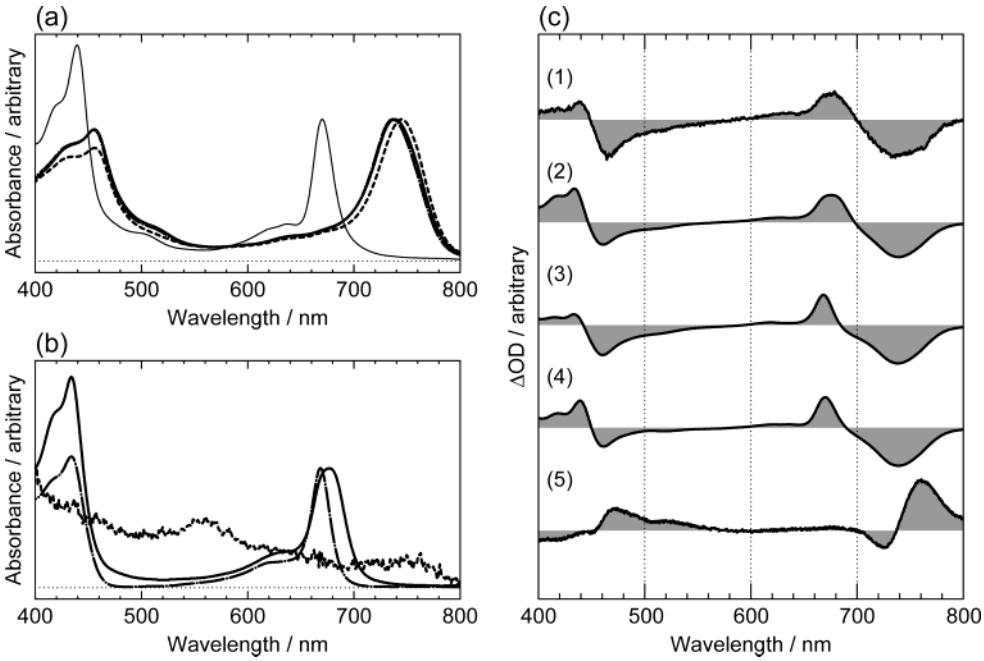

Figure 1. (a) Ground-state absorption spectra for native chlorosomes (thicker solid line), Car-depleted chlorosomes (broken line), reduced chlorosomes (dotted-broken line), and native chlorosomes after 1-hexanol treatment (thinner solid line). Nitrogen-bubbled or air-bubbled chlorosomes exhibited exactly the same absorption spectra as that of native chlorosomes. (b) Ground-state absorption spectra of BChl *c* monomer in methanol solution (dotted-broken line), the BChl *c* dimer in methylene chloride (solid line), and BChl *c* monomer in the T_1 state (broken line). (c; 1) The time-resolved spectrum (a difference spectrum of pump−probe minus probe only) of chlorosomes at 10 μs after excitation with extremely high photon density, (2) a difference spectrum of the BChl *c* dimer minus native chlorosomes, (3) a difference spectrum of the BChl *c* monomer minus native chlorosomes, (4) a difference spectrum of 1-hexanol-treated native chlorosomes minus native chlorosomes, and (5) a difference spectrum of native chlorosomes minus reduced chlorosomes.

(a) BChl c Monomer in the Methanol Solution. Because methanol is a hexa-coordinating solvent, the BChl *c* molecule is in the monomeric form in this particular solvent.

(b) Native Chlorosomes. As described in Materials and Methods, the excited-state dynamics within the BChl *c* aggregate in the rod element should be mainly observed in the present chlorosome preparation.

(c) Car-Depleted Chlorosomes. Chlorosomes were prepared from the cells that were grown in a medium suppressing the carotenoid synthesis. As described in the Introduction, the carotenoid, chlorobactene, in natural chlorosomes can function as a quencher of triplet BChl *c*.[25]

(d) Reduced Chlorosomes. The previously described "native chlorosomes" have been shown to contain a trace of BChl *c* radical cation (see the Introduction); the radical cation was removed by addition of a strong reductant, dithionite.

(e) Native Chlorosome Suspension Bubbled with Nitrogen (Hereafter, Abbreviated as "Nitrogen-Bubbled Chlorosomes"). Because the large, cylindrical network of BChl *c* aggregates in chlorosomes is stabilized only by BChl *c*−BChl *c* intermolecular interactions, it may be partially disrupted by the mechanical agitation of bubbling.

(f) Native Chlorosome Suspension Bubbled with Air ("Air-Bubbled Chlorosomes"). We originally expected that the partial disruption of the chlorosome structure might be accompanied by further oxidation with atmospheric oxygen. In reality, no clear spectral difference from "nitrogen-bubbled chlorosomes" was found (vide infra).

Figure 1 compares the ground-state absorption spectra of the just described samples: Figure 1a shows that modified chlorosomes give rise to similar but slightly different spectral patterns in comparison to that of native chlorosomes; Car-depleted chlorosomes exhibit the Q_y absorption that is shifted substantially to the red, whereas reduced chlorosomes exhibit one that is shifted slightly to the blue. The bubbling of the native chlorosome suspension with either nitrogen or air caused practically no spectral changes at all; therefore, their absorption spectra are not presented. When native chlorosomes were treated with 1-hexanol,[26] a spectrum suggesting a mixture of monomer and dimer emerged. Figure 1b shows that the Soret and the Q_y absorptions of the BChl *c* monomer in methanol and dimer in methylene chloride are shifted to the blue in comparison to those of chlorosomes. In the dimer, the relative intensity of Soret absorption is strongly enhanced and the Q_y absorption becomes broader, when compared to those in the monomer. (The result supports the previous idea that the 1-hexanol treatment gives rise to a mixture of monomer and dimer.) Upon triplet excitation, monomeric BChl *c* gives rise to a broad absorption with a peak around 560 nm and a monotonic increase in intensity toward 400 nm.

(B) Excited-State Reactions upon Excitation of the Cylindrical Aggregate with a Large Number of High-Energy Photons. Figure 2 shows the energy diagrams of BChl *c* in monomer and in native chlorosomes. After photoexcitation at 355 or 397 nm (see two weak horizontal lines), the BChl *c* molecules free in the solution or bound to chlorosomes are supposed to relax to the Soret state, then to the Q_x and the Q_y states, and eventually, to the ground state. Radiative transitions from those singlet states to the ground state are all allowed and give rise to fluorescence (spontaneous emission) in the absence of a radiation field. However, during the measurement of the time-resolved spectra, the white-continuum probing pulse always contains a spectral component to stimulate the radiative transition from each of those excited states. After analyzing all the time-resolved spectra of monomer and chlorosomes, it turned out that "stimulated emission" is actually the most efficient pathway of relaxation under the present experimental conditions.

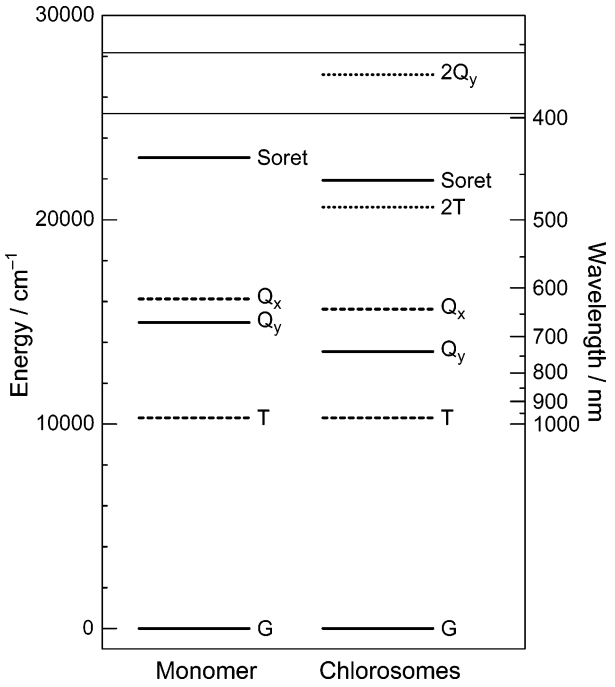

Figure 2. Energy diagrams for BChl *c* monomer (left) and chlorosomes (right). The energies of the Soret and the Q_y states were determined from the absorption spectra shown in Figure 1; those of the Q_x state were determined from a deconvolution of the shoulders on the high-energy side. The energy of the T state is transferred from that of Chl *a* having the same chlorin-conjugated system.[31] The energies of $2Q_y$ and 2T are shown for comparison. A pair of horizontal lines indicates the energies of photoexcitation, that is, 355 and 397 nm.

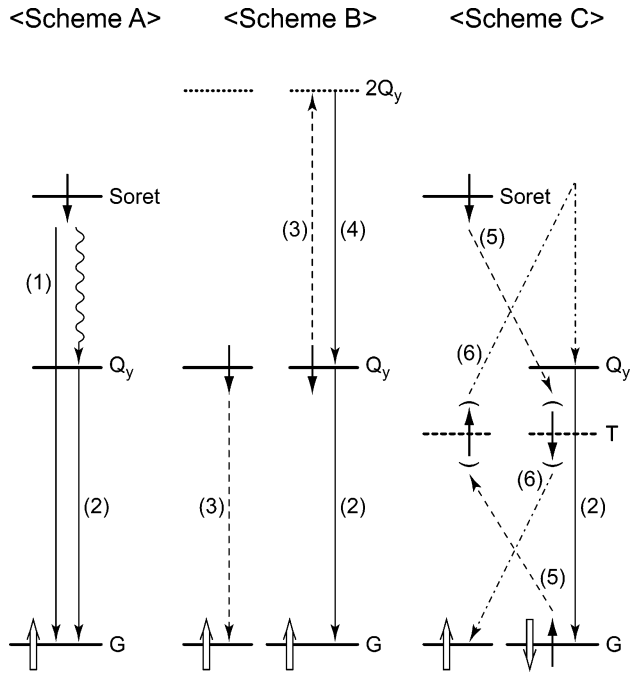

Figure 3. Main schemes of singlet- and triplet-energy dissipation. Scheme A: the direct Soret → G stimulated emission (1) and the Soret → Q_y internal conversion followed by the Q_y → G stimulated emission (2). Scheme B: Singlet−singlet annihilation (3) followed by the $2Q_y$ → Q_y stimulated emission (4) and the subsequent Q_y → G stimulated emission (2). Scheme C: A combination of singlet homofission (5) and triplet−triplet annihilation (6) followed by the Q_y → G stimulated emission (2). Short solid arrows indicate electron spins making transitions, while open short arrows indicate those that do not. The long straight and wavy arrows indicate radiative and nonradiative transitions, whereas a pair of long broken and dotted-broken arrows indicates resonant electronic transitions. The numbering corresponds to that of equations in the text.

This is most probably due to a very high population on the excited state and the presence of a radiation field.

In relation to the relaxation pathways, we focus on excited-state reactions[27] that can take place in the aggregate structure under the present experimental conditions. Figure 3 summarizes the schemes of the relevant excited-state reactions (note that the numbering in the figure corresponds to that in the following equations):

(i) Scheme A. Immediately after photoexcitation, one way of relaxation is stimulated emission from the Soret state,

$$\mathrm{S(Soret)} \rightarrow \mathrm{S(G)} + h\nu \qquad (1)$$

After the Soret → Q_y internal conversion (actually accompanying vibrational relaxation), stimulated emission from the Q_y state can also take place as another route of relaxation,

$$\mathrm{S(Q_y)} \rightarrow \mathrm{S(G)} + h\nu \qquad (2)$$

(ii) Scheme B. The singlet−singlet annihilation reaction can take place when the population of the Q_y state is high and a pair of the Q_y excitations interacts,

$$\mathrm{S(Q_y)} + \mathrm{S(Q_y)} \rightarrow \mathrm{S(2Q_y)} + \mathrm{S(G)} \qquad (3)$$

where another kind of stimulated emission, that is, the $2Q_y$ → Q_y stimulated emission, can take place,

$$\rightarrow \mathrm{S(Q_y)} + \mathrm{S(G)} + h\nu \qquad (4)$$

The resultant $S(Q_y)$ can give rise to additional stimulated emission.

(iii) Scheme C. The energy diagram in Figure 2 shows that the singlet homofission reaction can take place by electron exchange between a molecule in the Soret state and a neighboring molecule in the ground state to generate a pair of triplet states, that is,

$$\mathrm{S(Soret)} + \mathrm{S(G)} \rightarrow 2 \times \mathrm{T} \qquad (5)$$

When a pair of triplet excitations collides, the triplet−triplet annihilation reaction can take place,

$$2 \times \mathrm{T} \rightarrow \mathrm{S(Q_y)} + \mathrm{S(G)} \qquad (6)$$

(The energy diagram shows that the reverse reaction of eq 5 cannot take place energetically.) This process can give rise to delayed stimulated emission from the Q_y state. It is to be noted that each of the singlet−singlet and the triplet−triplet annihilation reactions (eqs 3 and 6) is a bimolecular reaction.

In the just described excited-state dynamics, we focused on the stimulated-emission processes because we will find those in the time-resolved spectra. However, nonradiative transitions including internal conversion and vibrational relaxation should be also taking place in parallel. Those internal-conversion and vibrational-relaxation processes give rise to thermal energy. The resultant heat may loosen the aggregate structure in a longer time scale.

In the present time-resolved absorption spectroscopy, we applied a large number of high-energy photons (see Materials and Methods). The number of photons applied per pulse *per BChl c molecule* can be estimated as follows on the basis of the number of photons and the number of BChl molecules in the beam waist. (i) Subpicosecond to nanosecond time-resolved absorption spectroscopy: in the "high photon-density" excita-

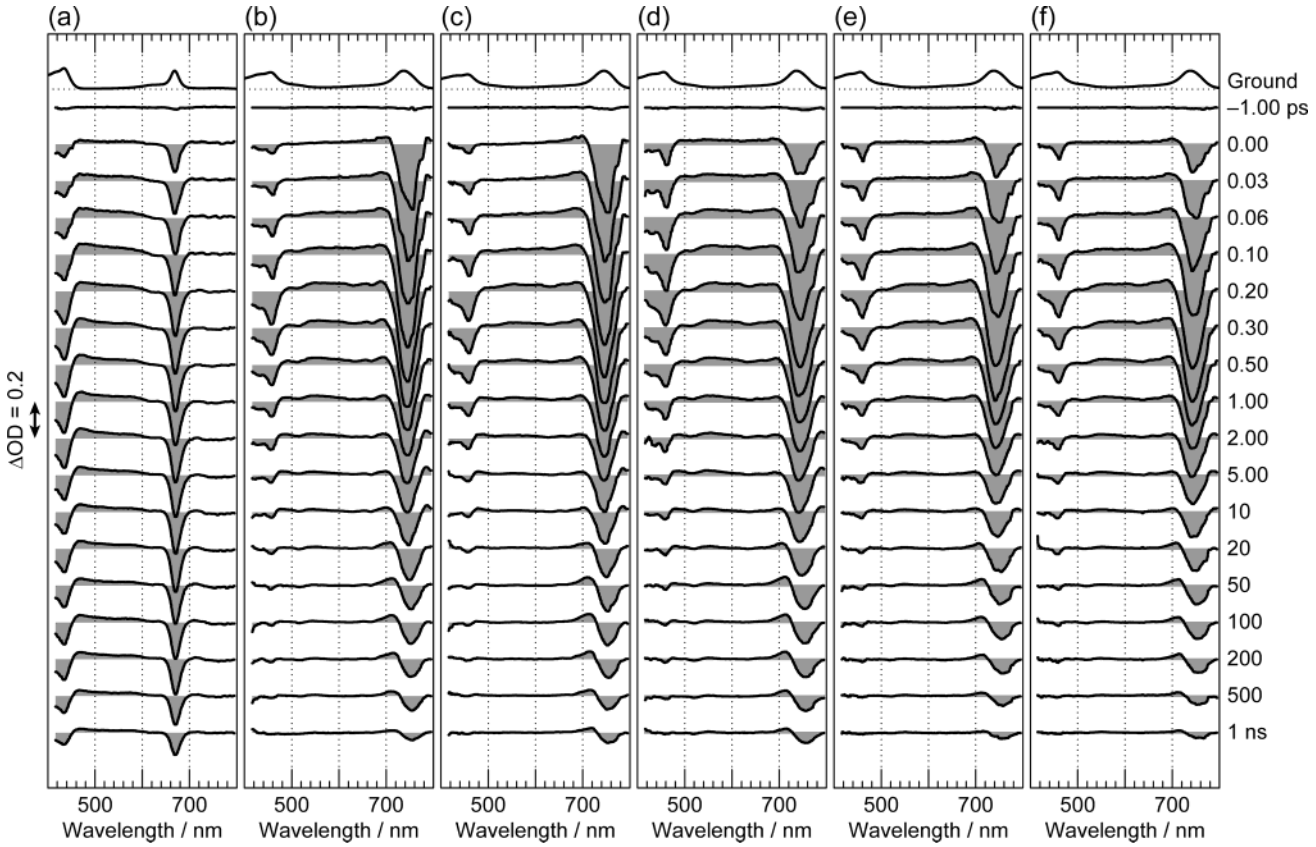

Figure 4. Time-resolved absorption spectra in the subpicosecond to nanosecond time region upon high photon-density excitation of BChl *c* monomer as well as native and modified chlorosomes: (a) Monomer in methanol solution, (b) native chlorosomes, (c) Car-depleted chlorosomes, (d) reduced chlorosomes, (e) nitrogen-bubbled chlorosomes, and (f) air-bubbled chlorosomes.

tion, 7×10^{-2} photon·pulse^{-1}·molecule^{-1}, whereas in the "low photon-density" excitation, 1×10^{-2} photon·pulse^{-1}·molecule^{-1}, for both the monomer in a solution and chlorosomes in a suspension. (ii) Submicrosecond to millisecond time-resolved absorption spectroscopy: in the excitation with "extremely high photon density", 3×10 photon·pulse^{-1}·molecule^{-1} for both the monomer in a solution and chlorosomes in a suspension. In the case of the rod element containing $\sim 10^3$ BChl *c* in the cylindrical aggregates,[3] the number of photons applied per pulse *per rod* would become 3 orders of magnitude larger.

It is most important to clearly differentiate photoexcitation under the physiological conditions and that under the present experimental conditions: Supposing that the integrated absorption cross section over the Soret and Q_y bands for the BChl *c* molecule is 1 Å^2 and that the intensity of sunlight (directly overhead at the equator on a clear day) is 2500 μE·m^{-2}·s^{-1}, the number of photons to be absorbed by the molecule turns out to be 15 photon·s^{-1}·molecule^{-1}. When the number of BChl *c* molecules in the rod is supposed to be 2000, the number of photons absorbed per rod becomes 3.0×10^4 photon·s^{-1} (see ref 28, for example). The light intensity to grow *Chl. tepidum* would be at least 1 order of magnitude lower. This calculation is concerned with the continuous wave white light from the sun. Here, the continuous, incoherent, and single-photon excitation to various vibronic states is taking place. The average time between photon absorption is infinitely long when compared to the time scales of excited-state reactions, if any.

In the present experiment of what we call "high-photon density" excitation, that is, 4×10^{14} photon·cm^{-2}·pulse^{-1} (see Materials and Methods), an estimation of the projected area of a rod of 10×100 nm^2 (side view)[3] and the repetition rate of 1 kHz lead to a number of photons possibly absorbed per rod, 4×10^6 photon·s^{-1}, which is 2 orders of magnitude larger than the previous estimation. Here, it is important to note that the actual irradiation time is as short as 0.1×10^{-12} s $\times$ 1000 = 10^{-10} s out of 1 s, for example. This calculation is concerned with the pulsed, monochromatic light from a laser. Here, the pulsed, coherent, and multiphoton excitation to a specified vibronic state is taking place; the excess photons would pass through the rod without any interaction (the rod can became transparent for them), leaving a saturated excitation. The excited-state reactions should take place immediately after this saturating excitation within an extremely short period of time.

Excited-State Dynamics in Chlorosomes As Probed by Subpicosecond to Nanosecond Time-Resolved Absorption Spectroscopy: (A) High Photon-Density Excitation. *(1) Characterization of Time-Resolved Spectra.* Figure 4 shows the subpicosecond to nanosecond time-resolved absorption spectra for a set of six samples characterized in subsection A of the previous section. Before getting into detailed characterization of the time-resolved spectra, the method how to differentiate stimulated emission from the bleaching of the ground-state absorption will be briefly mentioned. Although both of them give rise to negative signals in a difference absorption spectrum ("after" minus "before" photoexcitation), their patterns are quite different. We take the time-resolved spectra of native chlorosomes (Figure 4b), for example: The bleaching signal should keep exactly the same profile (the relative intensity of the Soret and Q_y absorption bands and their peak patterns), except for the sign, as the ground-state absorption spectrum shown on the top of the time-resolved spectra. Therefore, the sharp negative signal at 460 nm, on the top of the bleaching of the Soret absorption that reaches to a maximum at 0.20 ps, can be regarded as the signal of stimulated emission from the Soret

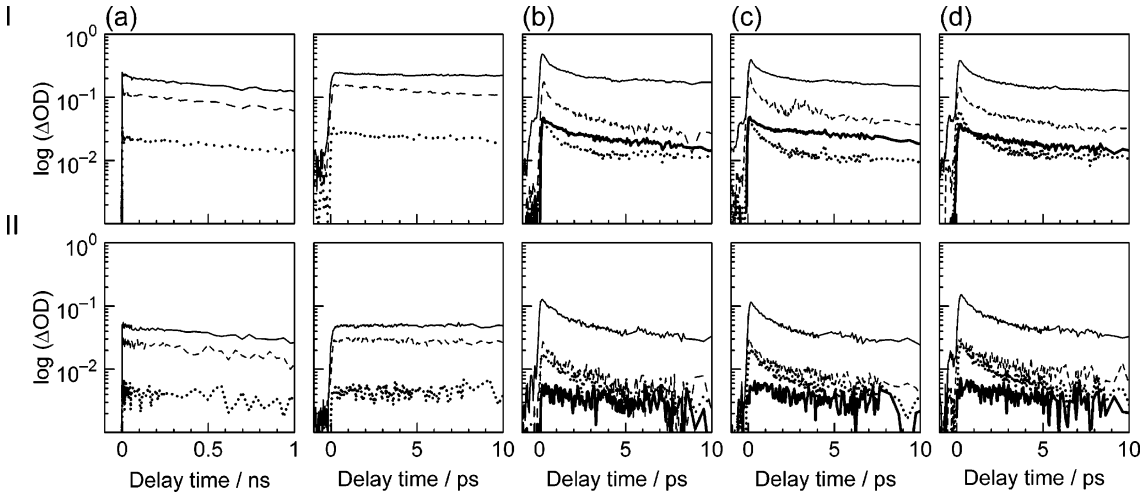

Figure 5. Time profiles showing the excited-state dynamics upon (I) high photon-density excitation and (II) low photon-density excitation. The following specific wavelengths are used. *(a) Monomer*: 430 nm, the bleaching of the Soret ← G absorption and the Soret → G stimulated emission (broken line); 570 nm, the $S_n \leftarrow Q_y$ transient absorption (dotted line); and 670 nm, the bleaching of the $Q_y \leftarrow$ G absorption and the $Q_y \rightarrow$ G stimulated emission (weak solid line). *(b) Native chlorosomes, (c) reduced chlorosomes, and (d) nitrogen-bubbled chlorosomes*: 460 nm, the bleaching of the Soret ← G absorption and the Soret → G stimulated emission (broken line); 550 nm, the $T_n \leftarrow T_1$ transient absorption (strong solid line); 680 nm, the $S_n \leftarrow Q_y$ transient absorption (dotted line); and 750 nm, the bleaching of the $Q_y \leftarrow$ G absorption and the $Q_y \rightarrow$ G stimulated emission (weak solid line).

state. A signal around 750 nm appearing in the 0.00−0.50-ps region, whose intensity is extremely high in comparison to the negative signals in the Soret region, can be regarded as a signal of stimulated emission from the Q_y state. This signal stays even in the decapicosecond to nanosecond region, where the bleaching of the Soret absorption becomes negligible. This consideration leads us to the conclusion that stimulated emission contributes most to the negative signals in the Soret and Q_y regions of the time-resolved spectra.

On the basis of the considerations just described and in subsection B, spectral changes in each sample can be characterized as follows:

(a) Monomer. The spectral pattern is more or less similar throughout all the delay times except for the overall intensity changes. It consists of the bleaching of the Soret and the Q_y absorptions (hereafter, we call them simply "the Soret and the Q_y bleachings") and an excited-state transient absorption between. Comparison of the relative intensities of those negative signals to those of the positive Soret and Q_y absorptions (shown on top of the panel) reveals that an additional contribution of the $Q_y \rightarrow$ G stimulated emission (when it is apparent, we will call this "the Q_y stimulated emission") is present. This set of signals rises and decays monotonically, reflecting the Q_y excitation.

(b) Native Chlorosomes. Much more drastic time-dependent changes in the spectral pattern are seen in this aggregate: (i) Immediately after excitation (0.00−0.03 ps), an extremely strong Q_y stimulated emission appears at 756 nm. The Soret stimulated emission is much weaker (see the sharp peak on the top of the Soret bleaching), a fact that indicates that the Soret $\rightarrow Q_y$ internal conversion is extremely efficient (see Scheme A in Figure 3). A transient absorption around 700 nm can be assigned to the excitonic $S_n \leftarrow Q_y$ absorption of an aggregate structure; such an excitonic $S_n \leftarrow Q_y$ absorption has been well-documented in the case of the ring-type BChl *a* aggregate in the LH2 complexes from purple bacteria.[29] (ii) Subsequently (0.06−0.20 ps), stimulated emission that is slightly shifted to the blue (746 nm) grows and then merges to the above peak at 756 nm. This observation can be explained in terms of the singlet−singlet annihilation reaction that accompanies both the $2Q_y \rightarrow Q_y$ stimulated emission (746 nm) and then the $Q_y \rightarrow$ G stimulated emission (756 nm; see processes 4 and 2 of Scheme B); these stimulated emissions may be slightly different in energy. (iii) With a slight additional delay (0.20−0.50 ps), a new transient-absorption pattern emerges in the 450−650-nm region, accompanying a broad peak around 550 nm that can be associated with the $T_n \leftarrow T_1$ absorption shown in Figure 1b. The generation of the T_1 state indicates the presence of the singlet homofission reaction (process 5 of Scheme C). (iv) Later (1.0−10 ps), the Q_y stimulated emission decays together with the $T_n \leftarrow T_1$ absorption and the Soret bleaching. The decay of the triplet signal on this time scale can be explained only in terms of the triplet−triplet annihilation reaction (process 6 of Scheme C). (v) In the final stage (20 ps−1 ns), only a pair of positive and negative signals remains in the 680−780-nm region; they can be assigned to the $S_n \leftarrow Q_y$ absorption and the Q_y stimulated emission (process 2 of Scheme C), respectively. The negligibly small intensity of the Soret bleaching indicates that the population on the Q_y state is actually very small and that the intensities of the $S_n \leftarrow Q_y$ absorption and the Q_y stimulated emission are very high. This anomalous spectral pattern, which is seen not in the monomer but in all native and modified chlorosomes in this time range, remains to be explained. This is probably due to the excitonic excitation to the Q_y state in the aggregate. Note that the maximum of the Q_y stimulated emission is red-shifted (754 nm) as a result of the relatively high $S_n \leftarrow Q_y$ transient absorption.

(c) Car-Depleted Chlorosomes. The time-dependent spectral changes are the same as those of native chlorosomes within the limit of experimental error. We, therefore, conclude that no effects of the carotenoid, chlorobactene, occur in native chlorosomes in this time range (triplet BChl may not reach the carotenoid molecule before reaching ground-state BChl).

(d) Reduced Chlorosomes. The time-dependent spectral changes are similar to those of native chlorosomes except for the following: Just after excitation (0.00−0.10 ps), a more pronounced peak of stimulated emission from the Soret state appears possibly as a result of the removal of the radical cation (a quenching center) by the reductant and the resultant higher population on the Soret state. The much stronger $T_n \leftarrow T_1$ absorption indicates rapid generation of the T_1 state through

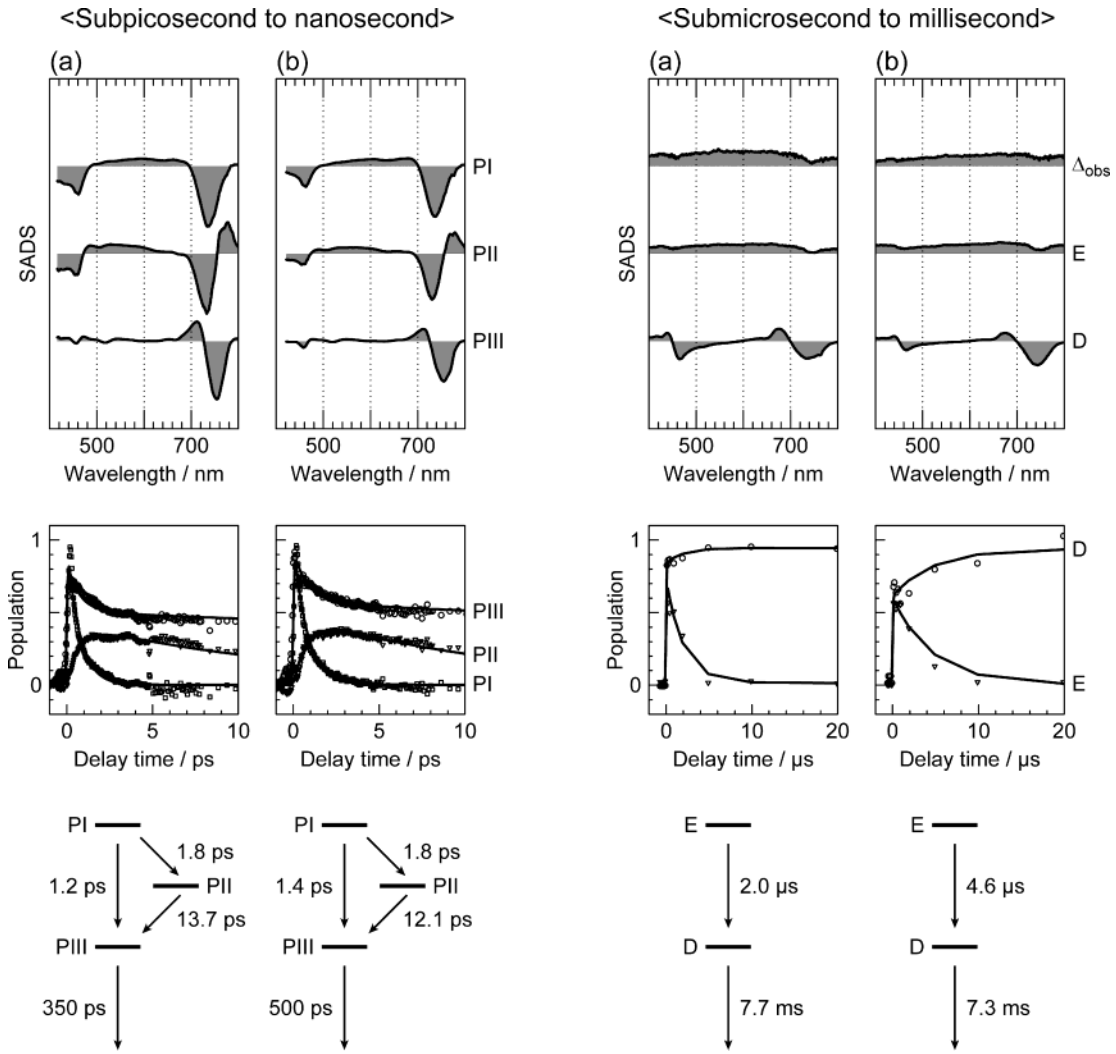

Figure 6. Results of SVD and global fitting of subpicosecond to nanosecond time-resolved spectra, on the left-hand side, for (a) native chlorosomes and (b) nitrogen-bubbled chlorosomes upon high photon-density excitation, and those of submicrosecond to millisecond time-resolved spectra, on the right-hand side, for (a) native chlorosomes and (b) nitrogen-bubbled chlorosomes upon excitation with extremely high photon density. The top and the second panels exhibit SADS and time-dependent changes in population, respectively. The models used for the global fitting are shown at the bottom together with the decay time constants.

the singlet homofission reaction (Scheme C, process 5); as a result, the initial Q_y stimulated emission (0.00 ps) becomes less pronounced.

(e) Nitrogen-Bubbled and (f) Air-Bubbled Chlorosomes. The time-dependent spectral changes are similar to those of native chlorosomes except for the following: Immediately after excitation (0.00−0.06 ps), stimulated emission from the lowest vibrational level of the Soret state becomes predominant. With a slight delay (0.20−0.30 ps), the Q_y stimulated emission reaches a maximum. The observation may be ascribable to a relatively higher population on the Soret state in the downsized aggregate structure (when compared to the case of the native chlorosomes).

(2) Characterization of Time Profiles. Figure 5 (I, upper panels) shows time profiles for the four selected samples including (a) monomer, (b) native chlorosomes, (c) reduced chlorosomes, and (d) nitrogen-bubbled chlorosomes. The time profiles can be characterized as follows:

(a) Monomer. When the logarithmic ordinate scale is used, all the time profiles at three different wavelengths exhibit a straight line (note the two different time scales), indicating a unimolecular decay of the Q_y excitation.

(b) Native Chlorosomes. The initial time profile at 680 nm (representing the $S_n \leftarrow Q_y$ absorption) exhibits a curve, a fact that indicates the presence of the bimolecular, singlet−singlet annihilation reaction (Scheme B, process 3). The initial time profile at 550 nm (the $T_n \leftarrow T_1$ absorption) also shows a nonlinear decay, indicating the presence of the bimolecular, triplet−triplet annihilation reaction (Scheme C, process 6). The initial, much faster decay in the $S_n \leftarrow Q_y$ absorption than that in the $T_n \leftarrow T_1$ absorption indicates the presence of the singlet homofission reaction, that is, the transformation of the Soret excitation into twice the T_1 excitation (Scheme C, process 5). The initial 460- and 750-nm time profiles (mainly representing the Soret and the Q_y stimulated emissions) exhibit much more pronounced nonlinear decay at the very initial state. Note that those two components rise and decay completely in phase.

(c) Reduced Chlorosomes. In comparison to native chlorosomes, the 680-nm profile (the $S_n \leftarrow Q_y$ absorption) exhibits an enhanced nonlinear decay, whereas the 550-nm time profile (the $T_n \leftarrow T_1$ absorption) exhibits a suppressed nonlinear decay, reflecting an enhanced singlet homofission reaction (Scheme C, process 5) under the reducing conditions. At the very initial stage, the 460-nm profile (the Soret stimulated emission) proceeds faster than the 750-nm profile (the Q_y stimulated emission), probably reflecting an enhanced initial population on the Soret state in the aggregate structure.

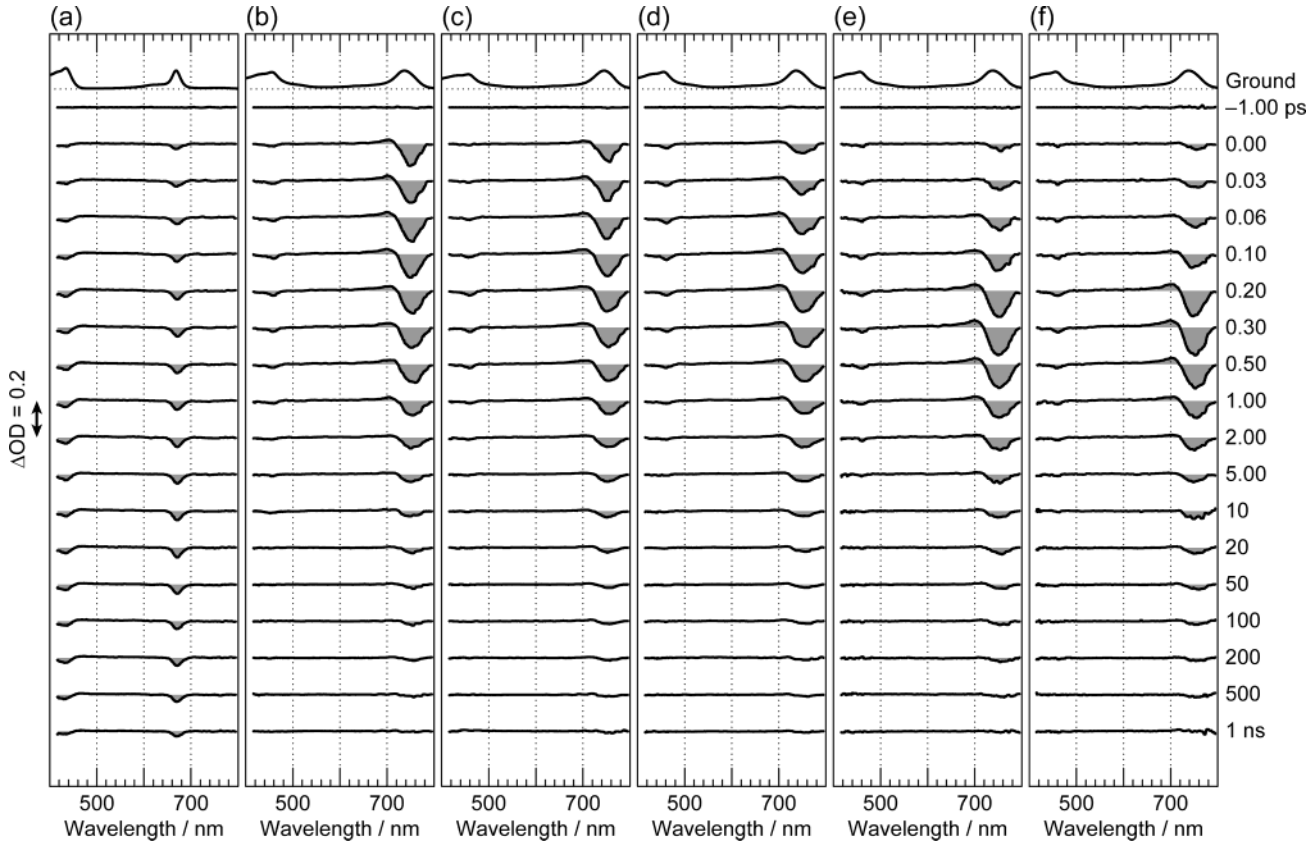

Figure 7. Time-resolved absorption spectra of BChl *c* monomer and native and modified chlorosomes in the subpicosecond to nanosecond time region upon low photon-density excitation. (a) Monomer in methanol solution, (b) native chlorosomes, (c) Car-depleted chlorosomes, (d) reduced chlorosomes, (e) nitrogen-bubbled chlorosomes, and (f) air-bubbled chlorosomes.

(d) Nitrogen-Bubbled Chlorosomes. Here again, the Soret stimulated emission initiates earlier than the Q_y stimulated emission most probably as a result of a smaller capacity of the downsized aggregate in accommodating the initial Soret excitation.

(3) SVD and Global Fitting. Figure 6 (panels on the left-hand side) shows the results of SVD and subsequent global fitting (see ref 24 and references therein) of the time-resolved spectra for the most typical two samples: (a) native chlorosomes and (b) nitrogen-bubbled chlorosomes. The top, the central, and the bottom panels exhibit species-associated difference spectra (SADS), time-dependent changes in the population, and decay schemes with time constants, respectively; temporally the first, the second, and the third phases are named PI, PII, and PIII.

(a) Native Chlorosomes. SADS (the top panel) can be characterized as follows: PI reflects the initial Soret and Q_y stimulated emissions overlapped with the Soret and Q_y bleachings and the transient absorption between. PII reflects both the $T_n \leftarrow T_1$ absorption that is generated by the singlet homofission reaction (Scheme C, process 5) and the $2Q_y \rightarrow Q_y$ (blue-shifted) and the $Q_y \rightarrow G$ stimulated emissions accompanying the singlet−singlet annihilation reaction (Scheme B). (The origin of the transient absorption on the red end is not clear.) PIII mainly reflects the $S_n \leftarrow Q_y$ transient absorption and the delayed Q_y stimulated emission due to a smaller number of the excitonic Q_y excitation. On the basis of the above assignment of PI, PII, and PIII, time-dependent changes in population (the central panel) and relevant time constants (the bottom panel) can be characterized as follows: The rapid decay of PI and the much slower decay of PIII reflect both the efficient Soret $\rightarrow Q_y$ internal conversion (Scheme A) and the singlet−singlet annihilation reactions (Scheme B). The rapid decay of PI and the accompanying rise of PII reflect the singlet homofission reaction (Scheme C, process 5). The faster decay of PII and the slower decay of PIII at the last stage (close to 10 ps) reflect the triplet−triplet annihilation reaction (Scheme C, process 6) and the resultant, delayed Q_y stimulated emission. The reaction scheme at the bottom shows the time constants of mutual transformations, which take place in the picosecond and decapicosecond time scales. Those time constants may be related to some of the decay time constants of the Q_y bleaching/stimulated emission reported previously.[13,30]

(b) Nitrogen-Bubbled Chlorosomes. The SADS of PI−PIII show the reduced intensities of the Q_y stimulated emission. The reduced time constant of the PII → PIII transformation suggests an accelerated triplet−triplet annihilation reaction. Both observations support the idea that the aggregate structure is downsized by the mechanical stress. Therefore, the same effect, irrespective of air/N_2 bubbling, is supported.

Thus, the empirical characterization of the time-resolved spectra has been verified by the results of the SVD and global-fitting analyses for the two typical samples.

(B) Low Photon-Density Excitation. *(1) Characterization of Time-Resolved Spectra.* Figure 7 shows the time-resolved spectra for the set of six samples upon low photon-density excitation, which can be characterized as follows:

(a) Monomer. The spectral pattern, consisting of the weak Soret and Q_y bleachings and an extremely weak, broad transient-absorption profile between, is conserved throughout the time-resolved spectra, an observation that indicates the rise and decay of the Q_y excitation.

(b) Native and (c) Car-Depleted Chlorosomes. The Q_y stimulated emission is extremely strong when compared to the negligibly weak Soret bleaching that represents the total excited-

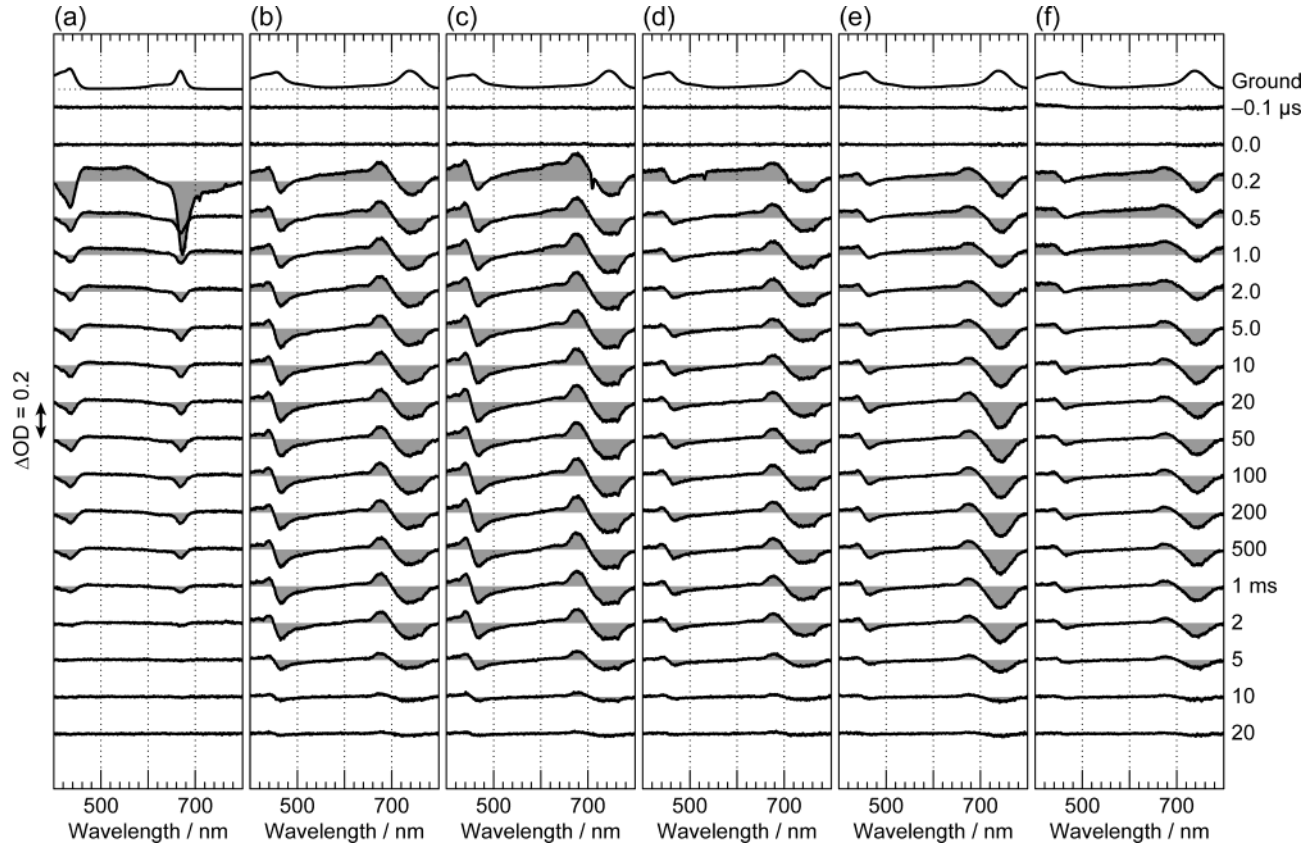

Figure 8. Time-resolved absorption spectra of BChl *c* monomer and native and modified chlorosomes in the submicrosecond to millisecond time region upon excitation with extremely high photon density. (a) Monomer in methanol solution, (b) native chlorosomes, (c) Car-depleted chlorosomes, (d) reduced chlorosomes, (e) nitrogen-bubbled chlorosomes, and (f) air-bubbled chlorosomes.

state population. This anomalous spectral pattern is basically the same as that observed in the last stage (0.5−1 ns) after high photon-density excitation (see Figure 4). The transient absorption peak at 700 nm can be assigned to the $S_n \leftarrow Q_y$ transient absorption of the aggregate structure. Upon low photon-density excitation, all the photon energy absorbed is mainly dissipated as the Q_y stimulated emission; its rapid decay suggests the presence of the singlet−singlet annihilation reaction (Scheme B).

(d) Reduced Chlorosomes. The much weaker Q_y stimulated emission immediately after excitation (0.00 ps) suggests an increased amount of the singlet homofission reaction (Scheme C, process 5). Also, the Soret stimulated emission can be seen more clearly. Both observations probably reflect a larger population on the initial Soret state as a result of the removal of radical cation (vide supra).

(e) Nitrogen-Bubbled and (f) Air-Bubbled Chlorosomes. Substantial suppression in the Q_y stimulated emission immediately after excitation suggests the presence of the singlet homofission (Scheme C, process 5) reaction. The enhancement of those reactions are probably due to the downsized aggregate structure.

(2) Characterization of Time Profiles. Figure 5 (II, lower panels) shows time profiles upon low photon-density excitation for the four typical samples, which can be characterized as follows:

(a) Monomer. Each time profile exhibits a horizontal line, indicating practically no decay at all in the shorter time range.

(b) Native Chlorosomes. The 550-nm time profiles (representing the $T_n \leftarrow T_1$ absorption) indicates the generation of a very small amount of the T_1 state; no clear triplet−triplet annihilation reaction is seen at all. The rest of the profiles exhibit nonexponential decay, indicating the presence of the singlet−singlet annihilation reaction (Scheme B).

(c) Reduced and (d) Nitrogen-Bubbled Chlorosomes. The 750-nm profile (representing the Q_y stimulated emission) exhibits slightly stronger nonlinearity, suggesting relatively a larger amount of the initial Soret population in those modified chlorosomes.

In summary, upon low photon-density excitation, the singlet−singlet annihilation reaction (Scheme B, process 3) takes place, but the triplet−triplet annihilation reaction (Scheme C, process 6) does not.

Partial Dissociation of Chlorosomes into the Piggy-Back Dimers Probed by Submicrosecond to Millisecond Time-Resolved Absorption Spectroscopy: Excitation with Extremely High Photon Density. *(1) Characterization of Time-Resolved Spectra.* Figure 8 shows the time-resolved absorption spectra of the set of six samples, upon excitation at 355 nm with "extremely high photon density" (3 orders of magnitude higher than the previous "high photon-density" experiments). We know that the application of such a high photon density is an extreme case. Even under those conditions, we had to accumulate a large number of spectral data to obtain a reasonably high S/N ratio (see Materials and Methods). The time-resolved spectra thus obtained for the six samples can be characterized as follows:

(a) Monomer. Immediately after excitation, extremely strong stimulated emission appeared on and below the position of the Q_y absorption (data not shown). Even the time-resolved spectrum at 0.2 μs (Figure 8a) exhibits strong Soret and Q_y stimulated emissions together with a strong transient absorption reminiscent of a mixture of the singlet and triplet excitations. The presence of stimulated emission in the submicrosecond time

regime indicated the contribution of triplet−triplet annihilation. The contribution of the excited-state absorption disappears within 10 μs, and the time-resolved spectrum converges into a spectral pattern consisting of the Soret and the Q_y bleachings with no contribution of stimulated emission (compare this spectrum to the ground-state absorption spectrum shown on the top). The spectral pattern decays in milliseconds.

(b) Native Chlorosomes. Immediately after excitation, a strong emission from the Q_y state took place on the lower energy side of the Q_y bleaching (data not shown). Here, no Soret stimulated emission took place contrary to the case of monomer, indicating again an extremely efficient Soret → Q_y internal conversion in the aggregate in chlorosomes. At 0.2 μs, a completely different spectral pattern appears, which is overlapped with a broad transient absorption ascribable to a mixture of the singlet and triplet excitations. The latter contribution then disappears, and only the new spectral pattern remains after 10 μs; the decrease in the contribution of the excited-state absorption is seen as the red shift of the zero-absorption point in the 500−600-nm region. This new spectral pattern was not seen at all in the time-resolved spectra in the subpicosecond to nanosecond time region.

(c) Car-Depleted Chlorosomes. The spectrum at 0.2 μs indicates that the initial generation of the excited-state absorption is strongly enhanced in this type of chlorosomes. This observation indicates that the carotenoid molecules in native chlorosomes function as a quencher of the triplet excited state through BChl-to-Car energy transfer in this submicrosecond time range, probably after efficient migration and collision of the BChl triplet excitations.

(d) Reduced Chlorosomes. In comparison to native chlorosomes, reduced chlorosomes generate a larger amount of the excited states as a result of the removal of the radical cation by the reducing agent.

(e) Nitrogen-Bubbled and (f) Air-Bubbled Chlorosomes. In comparison to native chlorosomes, the initial generation of the excited states seems to be slightly enhanced. This observation may reflect again the reduced size of the aggregate structure in this type of chlorosomes.

(2) Assignment of the New Spectral Pattern. Figure 1c shows (1) the time-resolved absorption spectrum of native chlorosomes at 10 μs after excitation (taken from Figure 8b) and a set of difference spectra of (2) dimer in methylene chloride minus native chlorosomes, (3) monomer in methanol minus native chlorosomes, (4) chlorosomes completely dissociated by 1-hexanol treatment minus native chlorosomes, and (5) native chlorosomes minus reduced chlorosomes. Comparison of the time-resolved spectrum of native chlorosomes with the set of difference spectra shows that the difference spectrum of dimer minus native chlorosomes is in the best agreement with it. (The relatively high positive absorption above 450 nm in the difference spectrum originates from the intense Soret absorption of dimer in solution.) More specifically, the round positive Q_y absorption around 680 nm of dimer (spectrum 2) fits to the time-resolved spectrum of chlorosomes much better than the sharp positive absorption of monomer (spectrum 3) or a slightly shorter positive absorption due to a mixture of the monomeric and dimeric forms obtained by the 1-hexanol treatment (spectrum 4). Native chlorosomes minus reduced chlorosomes (spectrum 5) does not explain the time-resolved spectrum at all. These results definitely indicate that, upon excitation with extremely high photon energy, the aggregate structure of chlorosomes partially dissociates into the piggy-back dimers in the submicrosecond time regime. Figure 8b shows that the difference spectral pattern disappears almost completely within 20 ms, a fact that indicates that the dissociated dimers can be completely reassembled into the original aggregate structure of the rod.

(3) SVD and Global Fitting. Figure 6 (panels on the right-hand side) shows the results of SVD and global fitting of the submicrosecond to millisecond time-resolved absorption spectra for the typical two samples, that is, (a) native chlorosomes and (b) nitrogen-bubbled chlorosomes. For each sample, the top profile shows the observed difference spectrum of 0.2 minus 10 μs, representing the excited-state absorption (denoted as Δ_{obs}), one SADS representing the excited-state absorption with a very weak Q_y stimulated emission or bleaching (denoted as E), and the other SADS representing the partially dissociated chlorosomes (denoted as D).

(a) Native Chlorosomes. The flat feature of Δ_{obs} and E suggests a mixture of the singlet and triplet excitations as mentioned previously. Time-dependent changes in population indicate that the decay of the excited states synchronizes with the rise of the dissociated state. The result strongly suggests that the excess excited-state energy, which is transforming into the thermal energy through the internal-conversion and vibrational-relaxation processes, triggers the dissociation of the chlorosome aggregate into the piggy-back dimers.

(b) Nitrogen-Bubbled Chlorosomes. The SADS of the excited states of this type of chlorosomes is similar to that of native chlorosomes, but the SADS of the dissociated state exhibits a stronger contribution of the Q_y stimulated emission. The presence of this delayed stimulated emission may give rise to a slower transformation from the excited state to the dissociated state; thus, the time for the E → D transformation is approximately doubled. The results confirm the idea that the initial population on the Soret state becomes relatively higher in this downsized aggregate structure.

Thus, the results of SVD and global fitting have verified the previously mentioned, empirical characterization of the time-resolved spectra.

Dissipation of Excess Energy in the Cylindrical BChl *c* Aggregate. Under the present experimental conditions, the relaxation processes that accompany the dissipation of the excited-state and the thermal energies have turned out to vary depending on the time range and the amount of photons supplied: In the subpicosecond to nanosecond time range, the internal-conversion and the excited-state reactions followed by stimulated emission (in the presence of a radiation field) play major roles. The processes can be classified into three categories (see Figure 3): (1) internal conversion from the Soret state down to the Q_y state followed by the Q_y stimulated emission (Scheme A); (2) the singlet−singlet annihilation reaction among the Q_y excitations followed by the $2Q_y$ → Q_y and the Q_y → G stimulated emissions (Scheme B); and (3) the singlet homofission reaction to generate a pair of the triplet excitations and the triplet−triplet annihilation reaction followed by the delayed Q_y stimulated emission (Scheme C). All three processes took place upon the high photon-density excitation, whereas the third reaction was negligible upon the low photon-density excitation. These results give a positive answer to the first question addressed in the Introduction: "can the excited-state reactions actually serve as the mechanisms of efficient quenching of the singlet and triplet excited states?" Presumably, efficient migration of the delocalized, excitonic singlet and triplet excitations in the cylindrical BChl *c* aggregate should facilitate the singlet−singlet and triplet−triplet annihilation reactions.

Modified chlorosomes have provided us with additional insight into the mechanisms: In comparison to native chlo-

rosomes, reduced chlorosomes and nitrogen-bubbled or air-bubbled chlorosomes tend to exhibit a stronger stimulated emission from the Soret state and an enhanced generation of the T_1 state accompanying delayed stimulated emission from the Q_y state. This trend can be explained in terms of the ratio of the initial population on the Soret state versus the size of the aggregated structure. In reduced chlorosomes, the number of excitations should be relatively increased by removing the quenching centers (radical cation), whereas in nitrogen-bubbled or air-bubbled chlorosomes, the size of the aggregated structure is relatively reduced.

In the submicrosecond to millisecond time range, excitation with extremely high photon density caused a strong stimulated emission in the submicrosecond time regime followed by the reversible dissociation of the aggregate structure into the piggy-back dimers. The dissociation reaction starts within submicroseconds after excitation and the reassociation reaction finishes in tens of milliseconds. The results give a positive answer to the second question addressed in the Introduction: "is there any change in the aggregated structure as a mechanism of efficient dissipation of the thermal energy?"

The excited-state energies that could not be dissipated by stimulated emission need to be dissipated as heat in the processes of internal conversion and vibrational relaxation. It seems that the thermal energy loosens and dissociates the aggregate structure, which is stabilized by the BChl *c*−BChl *c* intermolecular interactions among the piggy-back dimers. The dissociation of the rigid, two-dimensional network of BChl *c* aggregates is expected to provide an additional vibrational degree of freedom to facilitate efficient dissipation of the thermal energy through various vibrational relaxations; the dissociated part may function as a heat sink. The partial dissociation should inhibit the coherent Q_y excitation and its efficient migration, which is crucial for the light-harvesting function.

Thus, it has been shown that the aggregate structure of the rod has the mechanisms of efficient dissipation of the excited-state and thermal energies under the present experimental conditions. Those observations were made when a large number of high-energy photons were applied or, in other words, under the nonphysiological conditions.

Acknowledgment. The authors would like to thank Prof. Hugo Scheer for reading the manuscript. This work has been supported by a grant from the Ministry of Education, Culture, Sports, Science and Technology (Open Research Center Project) and a grant from NEDO (New Energy and Industrial Technology Development Organization, International Joint Research Grant).

References and Notes

(1) Blankenship, R. E.; Olson, J. M.; Miller, M. In *Anoxygenic Photosynthetic Bacteria*; Blankenship, R. E., Madigan, M. T., Bauer, C. E., Eds.; Kluwer Academic Publishers: Dordrecht, 1995; Chapter 20.

(2) van Grondelle, R.; Dekker, J. P.; Gillbro, T.; Sundstrom, V. *Biochim. Biophys. Acta* **1994**, *1187*, 1.

(3) Olson, J. M. *Photochem. Photobiol.* **1998**, *67*, 61.

(4) Blankenship, R. E.; Matsuura, K. In *Light-Harvesting Antennas in Photosynthesis*; Green, B. R., Parson, W. W., Eds.; Kluwer Academic Publishers: Dordrecht, 2003; Chapter 6.

(5) Balaban, T. S.; Holzwarth, A. R.; Schaffner, K.; Boender, G.-J.; de Groot, H. J. M. *Biochemistry* **1995**, *34*, 15259.

(6) Holzwarth, A. R.; Schaffner, K. *Photosynth. Res.* **1994**, *41*, 225.

(7) van Rossum, B.-J.; Steensgaard, D. B.; Mulder, F. M.; Boender, G. J.; Schaffner, K.; Holzwarth, A. R.; de Groot, H. J. M. *Biochemistry* **2001**, *40*, 1587.

(8) Nozawa, T.; Ohmoto, K.; Suzuki, M.; Morishita, Y.; Madigan, M. T. *Bull. Chem. Soc. Jpn.* **1993**, *66*, 231.

(9) Mizoguchi, T.; Limantara, L.; Matsuura, K.; Shimada, K.; Koyama, Y. *J. Mol. Struct.* **1996**, *379*, 249.

(10) Wang, Z.-Y.; Umetsu, M.; Kobayashi, M.; Nozawa, T. *J. Am. Chem. Soc.* **1999**, *121*, 9363.

(11) Mizoguchi, T.; Hara, K.; Nagae, H.; Koyama, Y. *Photochem. Photobiol.* **2000**, *71*, 596.

(12) Savikhin, S.; Buck, D. R.; Struve, W. S.; Blankenship, R. E.; Taisove, A. S.; Novoderezhkin, V. I.; Fetisova, Z. G. *FEBS Lett.* **1998**, *430*, 323.

(13) Savikhin, S.; Zhu, Y.; Lin, S.; Blankenship, R. E.; Struve, W. S. *J. Phys. Chem.* **1994**, *98*, 10322.

(14) Miller, M.; Cox, R. P.; Gillbro, T. *Biochim. Biophys. Acta* **1991**, *1057*, 187.

(15) Blankenship, R. E.; Cheng, P.; Causgrove, T. P.; Brune, D. C.; Wang, S. H.-H.; Choh, J.-U.; Wang, J. *Photochem. Photobiol.* **1993**, *57*, 103.

(16) Aschenbrücker, J.; Ma, Y.-Z.; Miller, M.; Gillbro, T. In *Photosynthesis: Mechanisms and Effects*; Garab, G., Ed.; Kluwer Academic Publishers: Dordrecht, 1998; Vol. I, p 153.

(17) van Noort, P.; Zhu, Y.; LoBrutto, R.; Blankenship, R. E. *Biophys. J.* **1997**, *72*, 316.

(18) Wang, J.; Brune, D. C.; Blankenship, R. E. *Biochim. Biophys. Acta* **1990**, *1015*, 457.

(19) Wahlund, T. M.; Woese, C. R.; Castenholz, R. W.; Madigan, M. T. *Arch. Microbiol.* **1991**, *156*, 81.

(20) Foidl, M.; Golecki, J. R.; Oelze, J. *Photosynth. Res.* **1997**, *54*, 219.

(21) Arellano, J. B.; Psencik, J.; Borrego, C. M.; Ma, Y.-Z.; Guyoneaud, R.; Garcia-Gil, J.; Gillbro, T. *Photochem. Photobiol.* **2000**, *71*, 715.

(22) Zhang, J.-P.; Fujii, R.; Qian, P.; Inaba, T.; Mizoguchi, T.; Koyama, Y.; Onaka, K.; Watanabe, Y.; Nagae, H. *J. Phys. Chem. B* **2000**, *104*, 3683.

(23) Fujii, R.; Furuichi, K.; Zhang, J.-P.; Nagae, H.; Hashimoto, H.; Koyama, Y. *J. Phys. Chem. A* **2002**, *106*, 2410.

(24) Zhang, J.-P.; Inaba, T.; Watanabe, T.; Koyama, Y. *Chem. Phys. Lett.* **2000**, *331*, 154.

(25) Melø, T. B.; Frigaard, N.-U.; Matsuura, K.; Razi Naqvi, K. *Spectrochim. Acta, Part A* **2000**, *56*, 2001.

(26) Matsuura, K.; Olson, J. M. *Biochim. Biophys. Acta* **1990**, *1019*, 233.

(27) Swenberg, C. E.; Geacintov, N. E. In *Organic Molecular Photophysics*; Birks, J. B., Ed.; John Wiley & Sons: London, 1973; Vol. 1, Chapter 10.

(28) Blankenship, R. E. *Molecular Mechanisms of Photosynthesis*; Blackwell Science: London, 2002; Chapter 5.

(29) Pullerits, T.; Chachisvilis, M.; Sundstörm, V. *J. Phys. Chem.* **1996**, *100*, 10787.

(30) Pšenčík, J.; Polívka, T.; Němec, P.; Dian, J.; Kudrna, J.; Malý, P.; Hála, J. *J. Phys. Chem. A* **1998**, *102*, 4392.

(31) Dvornikov, S. S.; Knyukshto, V. N.; Solovev, K. N.; Tsvirko, M. P. *Opt. Spektrosk.* **1979**, *46*, 689.